Hyper-Reflective Foci in Intermediate Age-Related Macular Degeneration: Spatial Abundance and Impact on Retinal Morphology

Marlene Saßmannshausen,[1,2] Marc Vaisband,[3,4] Leon von der Emde,[1] Kenneth R. Sloan,[5] Jan Hasenauer,[3,6] Frank G. Holz,[1,2] and Thomas Ach[1,2]

[1]Department of Ophthalmology, University Hospital Bonn, Germany
[2]Grade Reading Center, University of Bonn, Germany
[3]Life & Medical Sciences Institute, University of Bonn, Germany
[4]Department of Internal Medicine III with Haematology, Medical Oncology, Haemostaseology, Infectiology and Rheumatology, Oncologic Center; Salzburg Cancer Research Institute - Laboratory for Immunological and Molecular Cancer Research (SCRI-LIMCR); Paracelsus Medical University, Salzburg, Austria, Cancer Cluster Salzburg, Austria
[5]Department of Computer Science, University of Alabama at Birmingham, Birmingham, Alabama, United States
[6]Helmholtz Center Munich – German Research Center for Environmental Health, Institute of Computational Biology, Neuherberg, Germany

Correspondence: Thomas Ach, Department of Ophthalmology, University Hospital Bonn, Venusberg-Campus 1, Bonn 53127, Germany; thomas.ach@ukbonn.de.

Received: June 23, 2022
Accepted: December 28, 2022
Published: January 27, 2023

Citation: Saßmannshausen M, Vaisband M, von der Emde L, et al. Hyper-reflective foci in intermediate age-related macular degeneration: Spatial abundance and impact on retinal morphology. *Invest Ophthalmol Vis Sci.* 2023;64(1):20. https://doi.org/10.1167/iovs.64.1.20

Purpose. The purpose of this study was to analyze spatially resolved structural changes at retinal locations in presence (+) or absence (−) of hyper-reflective foci (HRF) in eyes with subretinal pigment epithelium (RPE) drusen in intermediate age-related macular degeneration (iAMD).

Methods. Patients with IAMD ($n = 40$; mean age = 69.7 ± 9.2 [SD] years) and healthy controls ($n = 27$; 64.2 ± 9.0) underwent spectral-domain optical-coherence-tomography imaging and fundus-controlled perimetry testing. After reviewing retinal layer segmentation, presence of HRF was annotated and retinal layer thicknesses (RLTs) extracted using ImageJ. Localized RLTs were compared between +HRF and −HRF positions. Univariate mixed linear models were used to investigate associations among RLT, HRF presence, and HRF size.

Results. In iAMD eyes, a mean of 11.1 ± 12.5 HRF were detected with a peak abundance at 0.5 to 1.5 mm eccentricity to the fovea. At +HRF positions, outer nuclear layer (ONL; $P = 0.0013$, average difference = −12.4 µm) and retinal pigment epithelium drusen complex (RPEDC; $P < 0.0001$, +45.6 µm) thicknesses differed significantly compared to −HRF positions, even after correcting for accompanying drusen-related RPEDC layer thickening ($P = 0.01$). Mixed linear models revealed a significant association between increasing HRF area and decreasing ONL (association score = −0.17, $P < 0.0001$; 95% confidence interval [CI] = −0.22 to −0.11), and inner photoreceptor segments (IS) layer thicknesses (−0.08, $P = 0.005$; 95% CI = −0.14 to −0.03). Spearman rank correlation analysis yielded a significant correlation between total HRF area and mesopic ($P = 0.015$), but not scotopic ($P = 0.305$) retinal sensitivity losses.

Conclusions. Descriptive analysis of this study demonstrated a predominant distribution of HRF at a foveal eccentricity of 0.5 to 1.5 mm, whereas further refined topographic analysis revealed a significant ONL layer thinning in presence of HRF even after correction for sub-RPE drusen presence compared to lesions in absence of HRF. Longitudinal studies are further needed to analyze the prognostic impact as well as the role of HRF presence in the context of iAMD.

Keywords: retinal layer thickness (RLT), fundus-controlled perimetry, structural biomarkers, age-related macular degeneration (AMD), geographic atrophy (GA)

Age-related macular degeneration (AMD) is a multifactorial retinal disease and remains a major cause of irreversible vision loss in industrialized countries.[1,2] Although the neovascular late stage manifestation of this disease (neovascular AMD [nAMD]) can be treated to slow disease progression, effective targeted-oriented therapies are currently still lacking for early (eAMD) or intermediate AMD (iAMD) disease stages to delay progression towards late stage nAMD or geographic atrophy (GA).[3,4] Therefore, identification of new structural biomarkers as early outcome measures for disease progression is of immense importance in AMD research.[5,6]

Copyright 2023 The Authors

This work is licensed under a Creative Commons Attribution-NonCommercial-NoDerivatives 4.0 International License.

For AMD diagnostics, currently, a multimodal imaging approach has been established, including color fundus photography (CFP), spectral domain optical coherence tomography (SD-OCT), angiography with or without dye (OCT-angiography), and autofluorescence. SD-OCT is a noninvasive, fast, and repeatable high-resolution imaging modality that has increased our knowledge of AMD.[7] Previously, risk factors impacting AMD progression have been described (e.g. presence of subretinal pigment epithelium [RPE], drusen or subretinal drusenoid deposits [SDD], drusen progression and regression and development of atrophy [incomplete and complete RPE and outer retinal atrophy [iRORA, cRORA]).[5,8,9] In recent iAMD studies, presence of hyper-reflective foci (HRF) were shown to confer one of the greatest risks among other structural biomarkers, including drusen volume, internal hyporeflectivity within drusen, or presence of SDD for disease progression toward late-stage AMD.[10–14]

HRFs are believed to represent migrated RPE cells into the neurosensory retina separated from the origin RPE layer.[5] On CFP, HRF have been shown to correspond to focal hyperpigmentation,[5,15] whereas in SD-OCT imaging, HRFs present as hyper-reflective spots with similar or higher reflectivity as the RPE.[5] In a previous work using a Cirrus high-density (HD)-OCT, a three pixel threshold has been applied to define the minimum size of HRF lesions[12]; however, in different SD-OCT imaging devices with varying image resolution, analysis of lesion size based on pixels might be imprecise since consensus definitions of cutoff values for HRF detection have not been brought forward.[5,12,16] Additionally, occurrence of HRF has also been described in the context of other degenerative retinal diseases, although their precise histological nature is currently still under discussion.[17,18]

Within the context of AMD, immunohistochemistry studies of human AMD retinas further showed that migrating RPE undergoes phenotype and molecular transdifferentiation: while losing RPE specific proteins (RPE65 and CRALBP), HRF gain markers typical for immune cells (CD68/163).[19] Although this seems to be true for nonexudative AMD, in nAMD, HRF may comprise RPE cells and lipid-loaded cells (mostly microglia and macrophages).[20,21]

In the past years, SD-OCT imaging described additional characteristics of HRF in iAMD. In a cross-sectional analysis, Schuman et al. have detected HRF in 41% of iAMD eyes, with these HRF being located over or laterally to sub-RPE drusen, whereas no HRF were found in areas without sub-RPE drusen or in age-matched control eyes.[22] Furthermore, they found significant photoreceptor layer thinning in areas above sub-RPE drusen.[22] In 518 fellow eyes with early or iAMD of the HARBOR study, by applying a deep-learning based approach, Waldstein and coworkers described HRF to predominantly occur at the temporal side at 0.5 mm eccentricity to the fovea and to mostly occur in eyes developing macular atrophy rather than nAMD.[23] Functionally, HRF presence has been shown to be associated with delayed rod-mediated dark-adaption as well as worse low-luminance visual acuity in eyes with early and iAMD.[24]

Despite well characterized HRF in iAMD, both in vivo and in histology,[15,19,21,22,25] a precise spatially resolved analysis of morphological retinal changes at locations with and without HRF as well as the correlation of HRF size to localized retinal layer thicknesses has been lacking to date.

Therefore, the objective of this study was to use SD-OCT imaging to detect HRF lesions as well as to perform a spatially resolved analysis of topographical structural changes at retinal lesions with and without HRF presence in a large cohort of iAMD eyes.

Methods

Subjects

For this noninterventional, observational natural history study, patients and age-matched healthy controls were recruited at the Department of Ophthalmology, University Hospital Bonn, Germany. This study was approved by the ethics committee (University Hospital Bonn, #125/14) and all study procedures adhered to the Tenets of the Declaration of Helsinki. All participants provided informed consent after explaining the study's nature and possible consequences of participation in this study.

For study inclusion, patients had to be diagnosed with iAMD in the presence of large sub-RPE drusen (>125 µm) as shown by CFP and near-infrared (NIR) plus SD-OCT imaging in either eye in accordance to the Beckman classification.[26] Lesions of iRORA or cRORA according to the definitions of the Classification of Atrophy Meeting (CAM) were not present in any study eye.[6,8] Only one eye per patient was included for analysis. If both eyes of a patient were eligible for study inclusion, only the right eye was included to exclude any distortion due to cross-correlation. Patients presenting with SDD in the absence of sub-RPE drusen were not included in this study. In addition, only subjects with clear media, visual acuity of at least logMAR 0.2, as well as a stable fixation were enrolled in both patient and control arms. Age-matched healthy subjects without any signs for current or previous ocular diseases served as controls.

Exclusion criteria for both groups were: refractive errors >3 diopters spherical equivalent, any signs of anterior segment diseases, GA as determined in fundus autofluorescence (FAF) imaging, macular neovascularization (MNV), diabetic retinopathy, glaucoma, and inflammatory retinal diseases, as well as previous vitreoretinal surgery or laser treatment. If both eyes met the inclusion criteria, both were included.

Retinal Imaging Protocol

After pupil dilatation (0.5% tropicamide and 2.5% phenylephrine), subjects underwent a detailed and standardized retinal imaging protocol using the high-speed combined and simultaneous confocal scanning laser ophthalmoscopy (cSLO) plus SD-OCT (Spectralis HRA + OCT, Heidelberg Engineering, Heidelberg, Germany; digital imaging resolution 768 × 768 pixels) device. The imaging protocol further included infrared reflectance (IR, 30 degrees × 30 degrees), FAF (exc λ = 488 nm, em λ = 500–800 nm, minimum 15 frames), single horizontal and vertical combined cSLO + SD-OCT scans through the fovea (30 degrees, automated real-time [ART] mode, and minimum of 9 frames), a raster SD-OCT scan (30 degrees × 25 degrees, ART, minimum 9 frames, 61 B-scans, and distance 120 µm) as well as CFP imaging.

Fundus-Controlled Perimetry

For functional testing, fundus-controlled perimetry (FCP) was performed in patients and controls based on recently described protocols.[27] In brief, mesopic (Goldmann size III, 200 ms 4-2 strategy, background luminance 1.27cd/m^2,

3 degrees radius, and 1-pixel fixation ring) and scotopic FCP (Goldmann size V, 200 ms, 4-2 strategy, background luminance 0.0032 cd/m2, 3 degrees radius, and 1-pixel fixation ring) of the macular retina with a 56-stimuli point test grid (10 degrees × 10 degrees) centered on the fovea was performed in all subjects using the Nidek MP-1S (Nidek Technologies, Italy, Padova). For testing under scotopic light conditions, subjects were dark-adapted for 30 minutes before FCP testing. Dark-adaptation for FCP testing was performed in a separate examination room under full-darkened conditions. Furthermore, a filter selection test (use of neutral density [ND] filter 0.0 log unit, 1.0 log unit, and 2.0 log unit) was performed prior to the main scotopic examination to overcome the limited dynamic range of threshold values. As retinal sensitivity thresholds differ within the neutral density filters, only patients with the neutral density filter ND 2.0 were included for final analysis.

Multilayer Retinal Thickness Analysis

For multi-retinal layer thicknesses analysis, volumetric SD-OCT imaging data were segmented automatically using the device's internal software (Spectralis Viewer Module 6.3.2.0; Heidelberg Engineering Eye Explorer, Heidelberg, Germany). In addition, automatic retinal layer segmentation was reviewed in each of the 61 B-scans and manually corrected, if needed.

The herein used retinal layers were defined according to the retinal layer definitions by Staurenghi et al.[28]: the retinal nerve fiber layer (RNFL) ranged from the internal limiting membrane (ILM) to the RNFL/ganglion cell layer (GCL) border, the GCL from the RNFL/GCL border to the GCL/inner plexiform layer (IPL) border, the IPL from the GCL/IPL boundary to the IPL/inner nuclear layer (INL) border, the outer plexiform layer (OPL) from INL/OPL border to the OPL/ONL border, the ONL from the OPL/ONL border to the external limiting membrane (ELM) including the Henle fiber layer according to Sadigh et al.,[29] the inner photoreceptor segments (IS) from the ELM to band 2 (ellipsoid zone [EZ]), and the outer photoreceptor segments (OS) from the EZ to band 3 (interdigitation zone) or the retinal pigment epithelium. According to previous publications,[30,31] the retinal pigment epithelium drusen-complex (RPEDC) ranged from the apex of the RPE layer to the Bruch's membrane (BM) including sub-RPE drusen, SDDs, basal linear deposits, or basal laminar deposits, if present. Thickness maps for each retinal layer were generated as volumetric en face image maps and transferred as tab-delimited files to ImageJ (US National Institutes of Health, Bethesda, MD, USA)[32] for further analysis.

Pointwise Topographic Analysis of Retinal Layer Thicknesses at HRF Position

To account for laterality, rotation, and tilt of eyes within the different imaging modalities, retinal imaging data (e.g. volumetric en face retinal layers thickness maps) were stack registered to the en face IR image according to vessel bifurcations and the exact position of the foveal pit (absence of inner and outer nuclear layers). The exact foveal position was as delineated by the central SD-OCT scan through the foveola, using a custom-written ImageJ plugin (CreativeComputation, KS, https://sites.imagej.net/CreativeComputation/). For consistency, right eyes were mirrored to left eyes.

Then, each B-scan of the 61-volume SD-OCT was screened (minimum of 150% magnification) by one experienced medical reader (author M.S.) for the presence of HRF, which were defined as hyper-reflective lesions with a reflectivity equal or higher to the RPE reflectivity in the specific OCT scan as well as being clearly separated from the underlying RPE band. According to conventional reading center practices, for the qualitative grading, HRF were deemed as being present if the grader was >90% confident that HRF are present in the corresponding B-scan. In order to compare HRF lesions detected in this study to a previously applied cutoff value of a 3-pixel minimum size for HRF detection,[24] only HRF with an area >0.0001 mm^2 (corresponding to a size of ≥3 pixels) were included in this analysis. After screening for HRF presence, each HRF was then manually encircled with a polygon at 300% magnification in each B-scan using ImageJ (Supplementary Fig. S1B). In case of a challenging assessment of single HRF lesions in a highly enlarged image, image magnification was reduced for annotations. The transition of the hyper-reflective lesion to the surrounding hyporeflective gray area was defined as the boundary of the polygon (Supplementary Fig. S1C/D). For each annotated HRF, detailed data including the area (in μm^2), the position relative to the fovea, the retinal layer in which the HRF was detected, as well as the corresponding retinal layer thicknesses were then automatically extracted at the exact location of each annotated HRF using a self-customized ImageJ plugin (CreativeComputation, KS, https://sites.imagej.net/CreativeComputation/).

To correlate findings between locations with (+HRF) and areas void of HRF (–HRF) within one eye, –HRF locations were mirrored horizontally relative to the center of the fovea, and retinal layer thicknesses were extracted accordingly.

All extracted data were then transferred to an Excel sheet (Microsoft Excel 2019, Microsoft Corporation, Redmond, WA, USA) for further data processing.

Statistical Analysis

Statistical analysis was performed using Python (Python Software Foundation, Wilmington, DE, USA, version 3.10.5). For the retinal layer thickness analysis, thicknesses were normalized to z-scores with respect to the mean and standard deviation of retinal layer thicknesses at the equivalent position in normal age-matched controls.

Retinal layer thicknesses between +HRF and –HRF locations were evaluated using the non-parametric paired Wilcoxon signed-rank test, as implemented in the Pingouin package for Python.[33] The results are reported as effect size, given by the rank-biserial correlation (RBC), and P values (corrected for multiple testing using the Bonferroni method). The significance threshold was chosen to be 0.05.

To investigate associations between retinal layer thicknesses and presence and size (e.g. area) of HRF lesions, linear mixed-effect modeling was utilized, because multiple HRFs per eye were evaluated and thus regular correlation analysis would have been invalid. For each layer, a univariate mixed linear model was fit to the data, with the z-transformed thickness as exogenous and z-transformed area as endogenous variable. The eye ID was used as the

Investigative Ophthalmology & Visual Science

grouping variable for the mixed-effect models. To account for intrasubject correlation, we have performed mixed-effect modeling, including the patient identity as a random effect.

For inner-eye control points (–HRF locations), HRF area was set to 0. The resulting model parameters are not precise correlation coefficients but are on the same scale and come with standard error estimates, yielding a *P* value to reject the null hypothesis that the true model coefficient is zero. To assess whether found effects persisted in a multivariate setting, we utilized conditional multivariate logistic regression (again using eye ID as the grouping variable). The covariates in the logistic regression were those for which a significant effect was observed in the univariate analysis.

For FCP analysis, data were normalized in terms of the point-wise sensitivity deviation (given in decibel [dB]) from the normative mean of the control group. Therefore, negative values signify a sensitivity loss and positive values supra-normal sensitivity values. Where applicable, numbers are reported as mean ± standard deviation. Spearman rank correlation was performed to analyze the association of the HRF area to mesopic and scotopic retinal sensitivity testing in patients.

Results

Demographics

Forty eyes of 40 patients with iAMD (mean age ± SD = 69.68 ± 9.24 years, median = 71.5, 0.25–0.75, interquartile range = 61–77.25, 18 men, and 9 pseudophakic eyes) and 29 control eyes of 27 control patients (64.2 ± 9.0, 0.25–0.75 interquartile range = 57–63, 24 men, and 4 pseudophakic eyes) were included. The mean best-corrected visual acuity was 0.096 logMAR (Snellen equivalent 20/25) in patients with iAMD and 0.03 logMAR (20/20) in healthy controls, respectively. Presence of SDD was found in 6 (15.0%) of 40 study eyes. In fellow eyes, signs for late-stage AMD were found in 13 eyes (n = 2 with GA and n = 11 with MNV), whereas 27 (67.5%) fellow eyes presented with iAMD. No HRF lesions were detected in healthy controls. Figure 1 presents a multimodal imaging patient example, and further details on the study cohort are given in Table 1.

Topographic HRF Distribution and HRF Morphology

In 40 study eyes, the mean number (±SD) of detected HRF was 11.1 ± 12.5 HRF, of which a mean of 8.6 ± 11.9 HRF

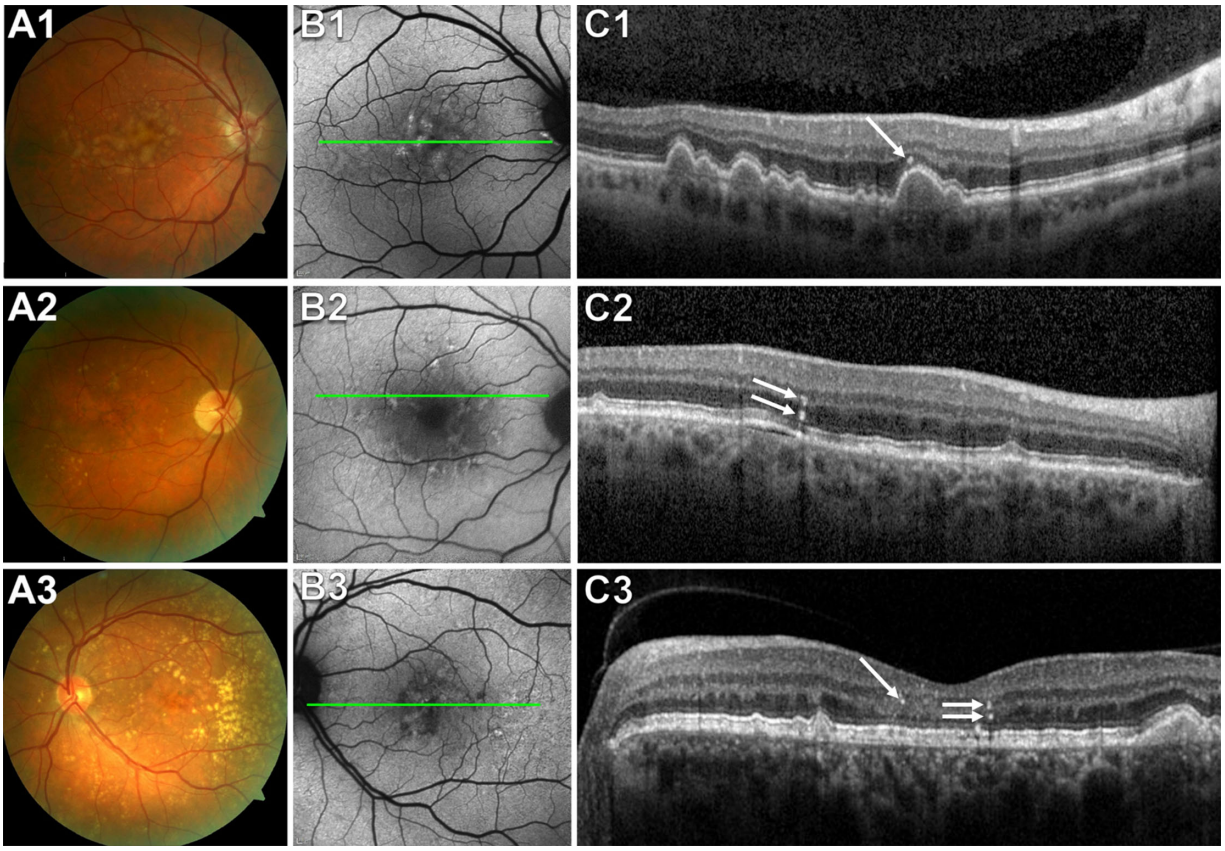

Figure 1. HRF in iAMD. Representative set of multimodal retinal imaging examples of patients with iAMD including color fundus photography (**A**), short wavelength fundus autofluorescence (**B**), and high-density spectral domain optical coherence imaging (SD-OCT) (**C**). The *green line* in panel **B** indicates the position of the corresponding SD-OCT B-scan. A1-C1 show a multimodal image example of a 55 year old patient with a typical lesion of a hyper-reflective focus (HRF; *white arrow*) within the outer nuclear layer (ONL) above a large sub-RPE druse. Figures A2 to C2 illustrate the example of a 56 year old patient with HRF with clearly detectable hyper pigmentary material in CFP imaging as well as simultaneous presence of sub-RPE drusen and subretinal drusenoid deposits (SDDs) in the OCT line scan. In addition, Figure A3 to C3 demonstrates another example of a 71 years-old in absence of a clear delineable lesion of geographic atrophy (>0.05 mm^2) in FAF imaging with presence HRF lesions positioned in the ONL close to the Henle Fiber layer.

Investigative Ophthalmology & Visual Science

Table 1. Study Cohort Characteristics

Characteristics	iAMD Patients (n = 40)	Controls (n = 29)
Age, y	69.68 ± 9.24	64.2 ± 9.0
Gender		
M	18	24
F	22	5
Eye		
Right	23	15
BCVA (logMAR)	0.096 ± 0.09	0.03 ± 0.06
Lens status		
Phakic	36	25
Pseudophakic	4	4

Results are presented as mean ± SD.
Abbreviation: iAMD, intermediate (i-) age-related macular degeneration.

were found directly above large sub-RPE drusen ($HRF_{RPEDC >2 SD}$), P = 0.0009). HRF showed a characteristic topographic pattern. The highest number of HRFs were observed at 0.5 to 1.5 mm eccentricity from the fovea with a mean number of 5.2 ± 7.3 HRFs per study eye. With increasing distance to the fovea, the number of HRFs decreased to 2.7 ± 5.6 HRF at an eccentricity of 1.5 to 3.0 mm and to 0.5 ± 2.5 HRFs at an eccentricity >3 mm from fovea, respectively. Considering only HRF above large sub-RPE drusen ($HRF_{RPEDC >2 SD}$), there was a similar topographic distribution with the highest HRF presence found at an eccentricity of 0.5 to 1.5 mm from the fovea (4.6 ± 7.3 HRF/eye; Fig. 2). No significant differences were found for HRF located nasally or temporally to the fovea (Table 2). Fifty-six percent of all detected HRFs were found in the ONL layer, followed by 26% in the OPL and 18% in the photoreceptor layers (IS + OS), respectively.

Retinal Layer Thickness at +HRF Locations

For the following analysis, no lesions of iRORA and cRORA were present in any included study eye. When considering topographically corrected retinal layer thicknesses for the remaining +HRF locations, within iAMD study eyes, the ONL was significantly thinner ($p_{corrected}$ = 0.0115, RBC = −0.687, average difference in retinal layer thickness = −12.38 µm), whereas the RPEDC layer was significantly thicker ($p_{corrected}$ = 0.0007, RBC = 0.844, average difference in retinal layer thickness +45.60 µm) at +HRF locations when compared with locations without HRF (–HRF). Even after accounting for the accompanying RPEDC thickness increase in presence of sub-RPE drusen, ONL layer thickness was still significantly thinner at +HRF than −HRF locations in the conditional logistic regression (P = 0.0105).

For the photoreceptor layers including IS (thickness differences = −1.24 µm) and OS (+0.58 µm) as well as for the OPL layer (+0.22 µm), no significant differences in retinal layer thicknesses at +HRF versus –HRF locations were found, respectively $p_{corrected}$ = 1.0; Table 3).

Correlation of Retinal Layer Thicknesses and HRF Size

Linear mixed-effect modeling further exhibited a significant association between an increasing HRF area (on SD-OCT B-scan) and a decreasing retinal layer thickness of the ONL layer (association score = −0.17, $p_{corrected}$ < 0.0001, 95% confidence interval [CI] = −0.22 to −0.11) as well as an increasing thickness of the RPEDC layer (association score 0.26, $p_{corrected}$ < 0.0001, 95% CI = 0.19 to 0.33). This analysis further revealed a significant association of an increasing HRF area to a localized IS layer thinning (association score = −0.08, $p_{corrected}$ = 0.041, 95% CI = −0.14 to −0.03). Detailed results of the univariate linear mixed models are shown in Table 4 as well as in Figure 3.

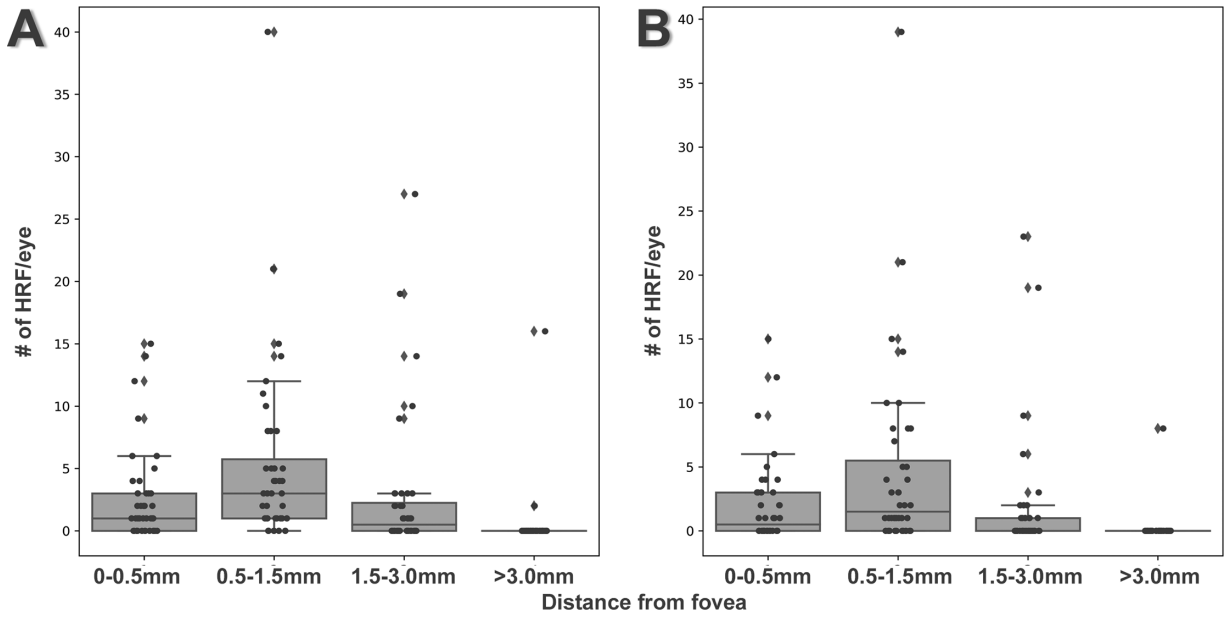

Figure 2. **HRF spatial distribution.** Boxplots demonstrating the topographic distribution of HRF in the complete study cohort (**A**) as well as for HRF overlying large sub-RPE drusen (**B**) (RPEDC thickness >2 SD). HRF are predominantly found at an eccentricity of 0.5 to 1.5 mm from the foveal center point, and less frequent at a foveal eccentricity of 0 to 0.5 mm, 1.5 to 3 mm, and >3 mm.

Investigative Ophthalmology & Visual Science

Table 2. Topographic Distribution of Hyper-Reflective Foci in Relation to the Fovea

Eccentricity	HRF	95% CI	HRF $_{RPEDC >2 SD}$	95% CI	*P* Value*	Nasal	95% CI	Temporal	95% CI	*P* Value*
Total	11.1 ± 12.5	1–31	8.6 ± 11.9	0–30	**0.0009**	5.1 ± 6.8	0–21	6.0 ± 7.3	0–22	0.6996
<0.5 mm	2.7 ± 3.7	0–12	2.1 ± 3.3	0–9	**0.0012**	1.6 ± 2.5	0–7	1.1 ± 1.9	0–5	0.0591
0.5–1.5 mm	5.2 ± 7.3	0–15	4.6 ± 7.3	0–15	**0.0005**	2.2 ± 3.3	0–8	3.1 ± 5.0	0–13	0.2070
1.5–3 mm	2.7 ± 5.6	0–14	1.8 ± 4.8	0–10	0.2576	1.2 ± 3.6	0–5	1.6 ± 3.0	0–8	0.1593
>3 mm	0.5 ± 2.5	0–0	0.2 ± 1.2	0–0	1.0000	0.3 ± 1.3	0–0	0.2 ± 1.2	0–0	1.0000

Topographic distribution of hyper-reflective foci (HRF) at different eccentricities from the foveal center point: <0.5 mm, 0.5–1.5 mm, 1.5–3 mm, and >3mm. Mean number of detected HRF is displayed for the total study cohort, for HRF overlying large sub-RPE drusen (RPEDC retinal layer thickness of >2 SD compared to healthy controls [HRF $_{RPEDC >2 SD}$]). Further, the mean number of HRF located nasally or temporally to the fovea is presented.

*Wilcoxon test. Significant values ($P < 0.05$) in bold.

All numbers are presented as mean ± standard deviation with the corresponding 95% confidence interval (95% CI).

Table 3. Comparison of Retinal Layer Thicknesses at +HRF versus –HRF Locations

Retinal Layer	Bonferroni Corrected *P* Value*	Difference in Retinal Layer Thickness, µm
RNFL	0.5665	+6.27
GCL	1.0	−1.34
IPL	1.0	+0.10
INL	1.0	−1.39
OPL	1.0	+0.22
ONL	**0.0115**	**−12.38**
IS	1.0	−1.24
OS	1.0	+0.58
RPEDC	**0.0007**	**+45.60**

Localized retinal layer thicknesses in presence (+HRF) and absence (−HRF) of HRF, after correction for retinal layer thicknesses of healthy controls. Negative values indicate that layers are thinner at +HRF positions.

*Wilcoxon test. Significant values in bold.

Abbreviations: RNFL, retinal nerve fiber layer; GCL, ganglion cell layer; IPL, inner plexiform layer; INL, inner nuclear layer; OPL, outer plexiform layer; ONL, outer nuclear layer; IS, inner photoreceptor segments; OS, outer photoreceptor segments; RPEDC, retinal pigment epithelium-drusen-complex; HRF, hyper-reflective foci.

Retinal Sensitivity in the Presence of HRF

For retinal sensitivity testing, overall pointwise retinal sensitivity deviation was −0.95 ± 3.04 dB (mean ± SD) for mesopic and −1.57 ± 3.19 dB for scotopic testing. Spearman rank correlation revealed a significant correlation between the total HRF area and the mesopic ($P = 0.015$), but not scotopic retinal sensitivity losses ($P = 0.305$).

Discussion

The main objective of this study was to describe the topographic distribution of HRF and to analyze spatially resolved retinal layer thicknesses at retinal locations in presence (+HRF) or absence of HRF (−HRF) in high-risk iAMD eyes. Within this study, +HRF in iAMD eyes were shown to predominantly occur parafoveally with a peak at a foveal eccentricity of 0.5 to 1.5 mm and to be less frequently detected with increasing distance to the foveal center point. Refined topographic retinal layer thickness analysis further revealed a significant ONL layer thinning at +HRF locations compared to −HRF locations even after correcting for a localized RPEDC layer thickening in presence of sub-RPE drusen or other sub-RPE material. These results underscore the prognostic impact of HRF as a biomarker for disease progression in iAMD.

In our study, a mean of 11 HRF/eyes were found in the macula OCT volume scan of eyes with iAMD which is higher than previously reported.[24] Echols et al. found only 2 HRFs in iAMD eyes but detected a mean of 20 hyper-reflective lesions with a size smaller than 3 pixels, termed as hyper-reflective specks, which were not observed in our study cohort.[24] The discrepancies might result from varying SD-OCT retinal imaging protocols (20 degrees × 15 degrees with 73 B-scan (Echols et al.) versus 30 degrees × 25 degrees 61 B-scans in this study), different image resolution scales of the imaging devices, or the subjective evaluation of reflectivity and the subsequent classification into spot or foci (with HRFs defined to be as reflective as the RPE). At the same time, single HRF lesions might have been double-counted in adjacent B-scans leading to varying numbers of HRF between studies. In addition, in both studies (Echols et al.[24] and the current study), subjects were classified as having iAMD in the study eyes. However, individual progression rates toward late-stage AMD and, therefore, prevalence rates for HRF lesions might differ between study cohorts. In fellow eyes of this study, evidence for late AMD in terms of GA or MNV development was observed in 13 eyes (32.5%), whereas no detailed information on the disease stage of fellow eyes was reported in the study by Echols et al.[24]

Sub-RPE drusen are abundant at the foveal center and within 1.5 mm of the foveola and appear to play an important role in the pathogenesis of HRF development. In our study, 66.6% of HRF were directly detected above large sub-RPE drusen with a RPEDC thickness >2 SD compared to controls. These findings support previous reports by Schuman et al. postulating HRF presence directly over or laterally to large (≥200 µm sub-RPE drusen.[22] Ho and colleagues further detected HRF directly above sub-RPE drusen in 73.3% of all study eyes with early or intermediate AMD.[16] In addition, analyzing HRF volumes using en face image slabs, Nassisi et al. found a significant positive correlation of HRF volume to drusen volume within 3 and 5 mm eccentricity to the fovea in early and iAMD eyes at baseline visit.[34] A focal thickening of tissue layers between the RPE and the choriocapillaris due to the deposition of material at the RPE's basal lamina (basal laminar deposit [BlamD]) and basal linear deposits (BLinD) and other drusen material in the sub-RPE space might lead to local hypoxia in the outer retina. This local hypoxia could further support the transition of RPE cells and subsequent anterior migration, then called HRF, into the outer retinal layers. In addition, focal hypoxia at +HRF locations above large sub-RPE drusen could further be negatively impacted by severe choriocapillaris flow deficit

Investigative Ophthalmology & Visual Science

Table 4. Univariate Linear Mixed-Effect Models

Parameter	Estimates (Association Coefficient)	Standard Error	*P* Value	95% Confidence Interval
RNFL				
(Intercept)	−0.140	0.060	0.020	−0.258 to −0.022
HRF area	0.040	0.031	0.205	−0.022 to 0.101
GCL				
(Intercept)	−0.152	0.062	0.015	−0.274 to −0.030
HRF area	−0.088	0.030	**0.004**	−0.148 to −0.029
IPL				
(Intercept)	−0.147	0.061	0.016	−0.267 to −0.027
HRF area	−0.029	0.030	0.330	−0.087 to 0.029
INL				
(Intercept)	−0.144	0.061	0.018	−0.263 to −0.025
HRF area	−0.005	0.029	0.855	−0.051 to 0.062
OPL				
(Intercept)	−0.145	0.061	0.018	−0.264 to −0.025
HRF area	−0.019	0.029	0.513	−0.077 to 0.038
ONL				
(Intercept)	−0.135	0.059	0.022	−0.250 to −0.020
HRF area	−0.165	0.030	**<0.0001**	−0.223 to −0.107
IS				
(Intercept)	−0.143	0.061	0.019	−0.262 to −0.023
HRF area	−0.080	0.028	**0.005**	−0.136 to −0.025
OS				
(Intercept)	−0.141	0.060	0.019	−0.260 to −0.023
HRF area	0.074	0.028	**0.009**	0.018 to 0.130
RPEDC				
(Intercept)	−0.108	0.058	0.060	−0.221 to 0.004
HRF area	0.257	0.036	**<0.0001**	0.186 to 0.328

Univariate linear mixed-effect model estimates for the localized change in retinal layer thicknesses with increasing HRF area [in μm^2], presented as association coefficients.

Abbreviations: RNFL, retinal nerve fiber layer; GCL, ganglion cell layer; IPL, inner plexiform layer border; INL, inner nuclear layer; OPL, outer plexiform layer; ONL, outer nuclear layer; IS, inner photoreceptor segments; OS, outer photoreceptor segments; RPEDC, retinal pigment epithelium drusen-complex.

in +HRF eyes and in particular directly below +HRF lesions, as shown in a recent study by Tiosano et al.[35]

Consequently, during the migration of RPE cells into the neurosensory retina one might expect alterations in retinal morphology on the level of photoreceptors segments despite for the ONL layer. However, in this study, no significant thickness changes of the IS and OS layers in +HRF versus –HRF locations were found, whereas there was a significant correlation between a decreasing IS layer thickness with an increasing HRF size. Notably, in another work, no significant differences in normalized EZ reflectivity between patients with and without HRF secondary to iAMD were found at the baseline visit.[34]

Only a few studies have elaborated in detail on retinal layer thicknesses in iAMD eyes and found a localized thickening of the RPEDC layer as well as a thinning of the outer retinal layers in presence of sub-RPE drusen,[22,36] also being associated with a localized loss of retinal function.[37,38]

More interestingly, in this study, the spatially resolved retinal layer thickness analysis also revealed a significantly thinner ONL layer at +HRF versus –HRF locations. This finding even remained significant after correcting for the accompanying RPEDC thickness increase in presence of sub-RPE drusen. In addition, because study eyes with the presence of iRORA and cRORA lesions were excluded prior for analysis, it seems that ONL layer thinning at +HRF locations is independent from RPEDC layer thickness. We, therefore, hypothesize that the presence of HRF precedes the localized cell loss and subsequent development of atrophy which can be tested in future long-term longitudinal high-resolution in vivo imaging studies examining retinal layers in early and iAMD while HRFs are present.

Localized ONL thinning further explains the stronger impairment of scotopic (although non-significant) than mesopic retinal sensitivity in these patients compared to healthy controls.[37,39] However, to what extent retinal sensitivity loss can really be attributed to the presence of HRF alone or to the presence of additional structural alterations in iAMD remains unclear at this point. Further, the direct spatially resolved correlation of +HRF positions to FCP stimuli points (in many cases, being larger than single HRF lesions) is limited. In this context, more detailed longitudinal structure-functional analysis assessing the impact of multiple iAMD associated risk factors (e.g. HRF, SDD, vitelliform lesions, refractile material, pigment epithelium detachment, and others) as well as retinal layer thickness to spatially resolved mesopic and scotopic retinal sensitivity is needed.

Correlating these structural findings with previous histological studies of a localized and more pronounced ONL thinning in presence of HRF lesions, it becomes obvious that HRF presence indicates degenerative disease-related alterations.[19,21,25] Interestingly, detailed clinical-histopathological correlations demonstrated that HRF detectable on OCT imaging migrating intraretinally toward inner retinal layers most likely correspond to abnormal RPE phenotypes undergoing a molecular transdifferentiation, epithelial to mesenchymal transformation (EMT), in which epithelial cells (like RPE) lose their apical-basal

Investigative Ophthalmology & Visual Science

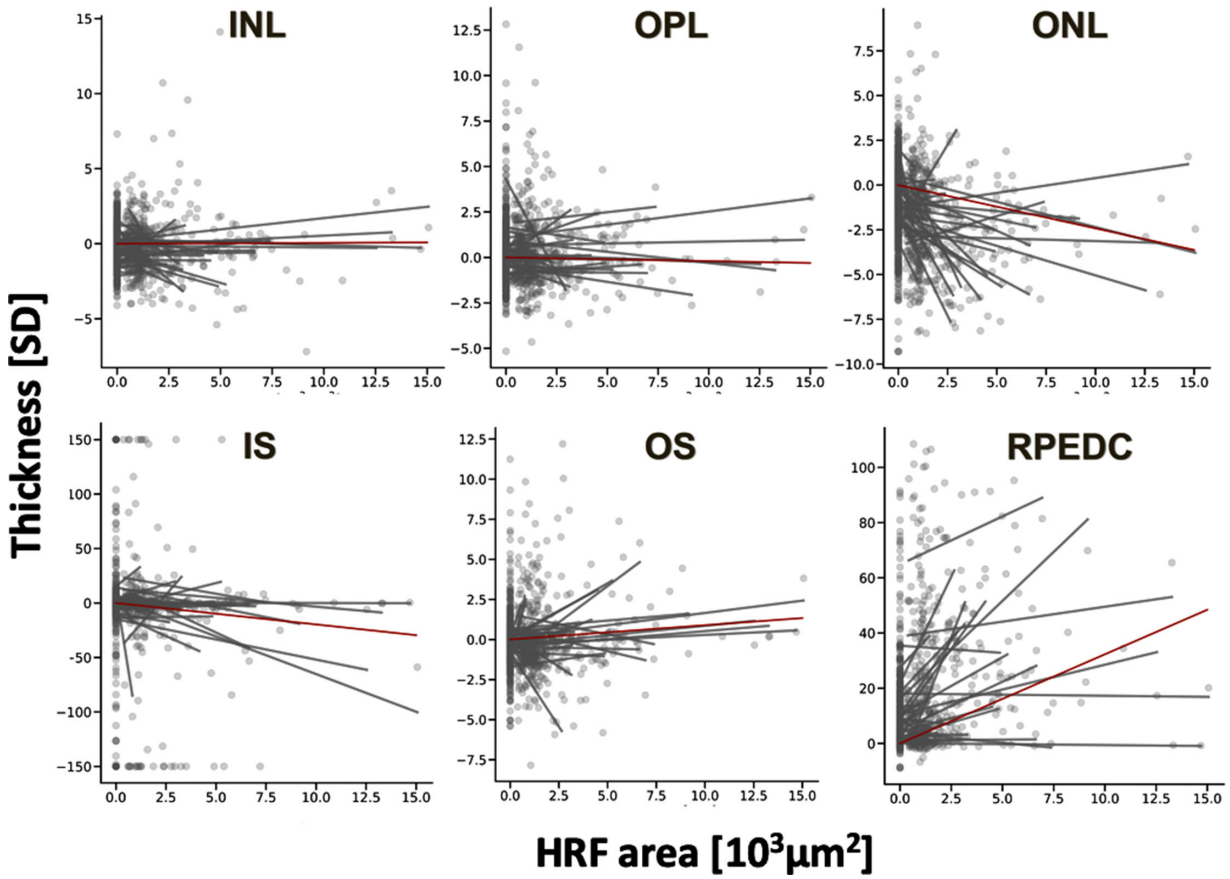

Figure 3. Correlation of retinal layer thicknesses with HRF size. Scatterplots showing the correlation of topographic retinal layer thickness changes (in standard deviations) for the inner nuclear layer (INL), the outer plexiform layer (OPL), the outer nuclear layer (ONL), and the inner (IS) and outer (OS) photoreceptor segments, as well as the retinal pigment epithelium drusen complex (RPEDC) in relation to the HRF area [in μm^2]. Individual measurement points are shown as *grey dots*, whereas the *grey lines* indicate linear regression slopes for individual eyes. The overall estimated relationship between increasing HRF area and changing retinal layer thickness as derived from the mixed-linear model is highlighted by a red line. Note: With increasing HRF area retinal layer thicknesses of the ONL ($P < 0.0001$) and the IS ($P = 0.005$) significantly decreased, whereas retinal layer thickness of the RPEDC ($P < 0.0001$) significantly increased.

polarity, modulate cytoskeleton, and further reduce their cell-cell adhesion in response to a larger stress, reduced vascular support due to age and disease-related loss of choroid and choriocapillaris resulting in progression toward retinal atrophy development.[19] However, future longitudinal studies with SD-OCT imaging with even higher resolution, and, therefore, a likely higher visibility of RPE changes are needed to detect and describe these dynamic cellular alterations in vivo in AMD eyes in more detail.

Our study has several limitations. First, the cohort of this study only included cross-sectional data from patients with iAMD being at a high risk for disease progression, which could have led to the high number of HRF detected in one eye. Second, the presence of various other structural parameters as vitelliform lesions, pigment epithelium detachment, and refractile deposits were not assessed in this study. Third, within the descriptive analysis of HRF lesions, in single cases, few HRF lesions might be counted more than once due to the presence of HRF lesions in adjacent OCT-B scans. In addition, larger HRFs can be well constrained based on the currently accepted definition (i.e, reflectivity compared to RPE), but there is not a 100% discrimination method to noise at this point, especially for the small HRFs. New technologies such as high-resolution OCT will further contribute to better discrimination in the future. Finally, lesions of HRF were annotated semi-automatically by one retina specialist, although highly experienced in standardized retinal imaging data analysis. However, strengths of this study include the use of a standardized retinal imaging protocol performed with the same imaging device with high-quality images for all subjects, the implementation of a software-based tool for a detailed topographic retinal layer thickness analysis at the spatially resolved retinal positions of +HRF, the prior exclusion of study eyes with evidence for early signs of retinal atrophy (e.g. presence of iRORA and cRORA), the comparison of retinal layer thickness at +HRF to –HRF locations, as well as the detailed point-wise correction of retinal layer thicknesses and retinal sensitivity values to healthy age-matched controls.

Future studies should include automated retinal image analysis tools to reliably assess HRF prevalence and structural alterations at +HRF locations within a longitudinal data set and to quantify these lesions. These approaches will further help to validate the impact of HRF as a biomarker for disease progression in large clinical trials.

In summary, while migrating into the inner retina, HRFs leave a trail of remodeling impacting retinal morphology and function. Localized RPEDC thickening with subsequent

Investigative Ophthalmology & Visual Science

ischemia and loss of nutrient supply may not only impact the outer retina but also lead to a localized ONL layer thinning. The presence of HRF is associated with a stronger thinning of ONL layer compared to retinal location with sub-RPE drusen in absence of HRF. These findings indicate the important role of HRF as an in vivo retinal imaging-based biomarker in iAMD.

Acknowledgments

The authors thank Verena Bonn for her administrative support in data acquisition and Ben Isselmann for his IT support in the retinal imaging data analysis.

Supported by the BONFOR GEROK Program, Faculty of Medicine, University of Bonn, Grant No. O-137.0030 (M.S.), the Anna-Katharina Eichenauer Foundation (M.S.), and the A. Döllner Foundation (M.V.).

Disclosure: **M. Saßmannshausen**, Heidelberg Engineering (F), Optos (F), Zeiss (F), CenterVue (F); **M. Vaisband**, None; **L. von der Emde**, None; **K.R. Sloan**, None; **J. Hasenauer**, Boehringer-Ingelheim (F); **F.G. Holz**, Acucela (C, F), Allergan (F), Apellis (C, F), Bayer (C, F), Boehringer-Ingelheim (C), Bioeq/Formycon (F, C), CenterVue (F), Ellex (F), Roche/Genentech (C, F), Geuder (C, F), Graybug (C), Gyroscope (C), Heidelberg Engineering (C, F), IvericBio (C, F), Kanghong (C, F), LinBioscience (C), NightStarX (F), Novartis (C, F), Optos (F), Oxurion (C), Pixium Vision (C, F), Oxurion (C), Stealth BioTherapeutics (C), Zeiss (F, C); **T. Ach**, Bayer (C), Roche (C), Novartis (C), Novartis (R), Heidelberg Engineering (C), Apellis Pharmaceuticals (C), Nidek (C, R)

References

1. Wong WL, Su X, Li X, et al. Global prevalence of age-related macular degeneration and disease burden projection for 2020 and 2040: a systematic review and meta-analysis. *Lancet Glob Health*. 2014;2:e106–e116.
2. Colijn JM, Buitendijk GHS, Prokofyeva E, et al. Prevalence of Age-Related Macular Degeneration in Europe: The Past and the Future. *Ophthalmology*. 2017;124:1753–1763.
3. Mitchell P, Liew G, Gopinath B, Wong TY. Age-related macular degeneration. *The Lancet*. 2018;392:1147–1159.
4. Fleckenstein M, Keenan TDL, Guymer RH, et al. Age-related macular degeneration. *Nat Rev Dis Primers*. 2021;7:31.
5. Jaffe GJ, Chakravarthy U, Freund KB, et al. Imaging Features Associated with Progression to Geographic Atrophy in Age-Related Macular Degeneration: Classification of Atrophy Meeting Report 5. *Ophthalmology Retina*. 2021;5:855–867.
6. Sadda SR, Guymer R, Holz FG, et al. Consensus Definition for Atrophy Associated with Age-Related Macular Degeneration on OCT: Classification of Atrophy Report 3. *Ophthalmology*. 2018;125:537–548.
7. Keane PA, Patel PJ, Liakopoulos S, Heussen FM, Sadda SR, Tufail A. Evaluation of age-related macular degeneration with optical coherence tomography. *Surv Ophthalmol*. 2012;57:389–414.
8. Guymer RH, Rosenfeld PJ, Curcio CA, et al. Incomplete Retinal Pigment Epithelial and Outer Retinal Atrophy in Age-Related Macular Degeneration: Classification of Atrophy Meeting Report 4. *Ophthalmology*. 2020;127:394–409.
9. Thiele S, Nadal J, Fleckenstein M, et al. Longitudinal Analysis of Drusen Volume in Intermediate Age-Related Macular Degeneration Using Two Spectral-Domain Optical Coherence Tomography Scan Patterns. *Ophthalmologica. Journal International D'ophtalmologie. International Journal of Ophthalmology. Zeitschrift fur Augenheilkunde*. 2018;239:110–120.
10. Christenbury JG, Folgar FA, O'Connell RV, Chiu SJ, Farsiu S, Toth CA. Progression of intermediate age-related macular degeneration with proliferation and inner retinal migration of hyperreflective foci. *Ophthalmology*. 2013;120:1038–1045.
11. Nassisi M, Lei J, Abdelfattah NS, et al. OCT Risk Factors for Development of Late Age-Related Macular Degeneration in the Fellow Eyes of Patients Enrolled in the HARBOR Study. *Ophthalmology*. 2019;126:1667–1674.
12. Lei J, Balasubramanian S, Abdelfattah NS, Nittala MG, Sadda SR. Proposal of a simple optical coherence tomography-based scoring system for progression of age-related macular degeneration. *Graefe's Arch Clin Exp Ophthalmol*. 2017;255:1551–1558.
13. Ouyang Y, Heussen FM, Hariri A, Keane PA, Sadda SR. Optical coherence tomography-based observation of the natural history of drusenoid lesion in eyes with dry age-related macular degeneration. *Ophthalmology*. 2013;120:2656–2665.
14. Sleiman K, Veerappan M, Winter KP, et al. Optical Coherence Tomography Predictors of Risk for Progression to Non-Neovascular Atrophic Age-Related Macular Degeneration. *Ophthalmology*. 2017;124:1764–1777.
15. Folgar FA, Chow JH, Farsiu S, et al. Spatial correlation between hyperpigmentary changes on color fundus photography and hyperreflective foci on SDOCT in intermediate AMD. *Invest Ophthalmol Vis Sci*. 2012;53:4626–4633.
16. Ho J, Witkin AJ, Liu J, et al. Documentation of intraretinal retinal pigment epithelium migration via high-speed ultrahigh-resolution optical coherence tomography. *Ophthalmology*. 2011;118:687–693.
17. Fragiotta S, Abdolrahimzadeh S, Dolz-Marco R, Sakurada Y, Gal-Or O, Scuderi G. Significance of Hyperreflective Foci as an Optical Coherence Tomography Biomarker in Retinal Diseases: Characterization and Clinical Implications. *J Ophthalmol*. 2021;2021:6096017.
18. Bolz M, Schmidt-Erfurth U, Deak G, Mylonas G, Kriechbaum K, Scholda C. Optical coherence tomographic hyperreflective foci: a morphologic sign of lipid extravasation in diabetic macular edema. *Ophthalmology*. 2009;116:914–920.
19. Cao D, Leong B, Messinger JD, et al. Hyperreflective Foci, Optical Coherence Tomography Progression Indicators in Age-Related Macular Degeneration, Include Transdifferentiated Retinal Pigment Epithelium. *Invest Ophthalmol Vis Sci*. 2021;62:34.
20. Li M, Dolz-Marco R, Messinger JD, et al. Clinicopathologic Correlation of Anti-Vascular Endothelial Growth Factor-Treated Type 3 Neovascularization in Age-Related Macular Degeneration. *Ophthalmology*. 2018;125:276–287.
21. Pang CE, Messinger JD, Zanzottera EC, Freund KB, Curcio CA. The Onion Sign in Neovascular Age-Related Macular Degeneration Represents Cholesterol Crystals. *Ophthalmology*. 2015;122:2316–2326.
22. Schuman SG, Koreishi AF, Farsiu S, Jung S, Izatt JA, Toth CA. Photoreceptor layer thinning over drusen in eyes with age-related macular degeneration imaged in vivo with spectral-domain optical coherence tomography. *Ophthalmology*. 2009;116:488–496.e2.
23. Waldstein SM, Vogl W-D, Bogunovic H, Sadeghipour A, Riedl S, Schmidt-Erfurth U. Characterization of Drusen and Hyperreflective Foci as Biomarkers for Disease Progression in Age-Related Macular Degeneration Using Artificial Intelligence in Optical Coherence Tomography. *JAMA Ophthalmol*. 2020;138:740–747.
24. Echols BS, Clark ME, Swain TA, et al. Hyperreflective Foci and Specks Are Associated with Delayed Rod-Mediated Dark Adaptation in Nonneovascular Age-Related Macular Degeneration. *Ophthalmol Retina*. 2020;4:1059–1068.
25. Curcio CA, Zanzottera EC, Ach T, Balaratnasingam C, Freund KB. Activated Retinal Pigment Epithelium, an

Optical Coherence Tomography Biomarker for Progression in Age-Related Macular Degeneration. *Invest Ophthalmol Vis Sci*. 2017;58:BIO211–BIO226.

26. Ferris FL, Wilkinson CP, Bird A, et al. Clinical classification of age-related macular degeneration. *Ophthalmology*. 2013;120:844–851.
27. Saßmannshausen M, Zhou J, Pfau M, et al. Longitudinal Analysis of Retinal Thickness and Retinal Function in Eyes with Large Drusen Secondary to Intermediate Age-Related Macular Degeneration. *Ophthalmol Retina*. 2021;5:241–250.
28. Staurenghi G, Sadda S, Chakravarthy U, Spaide RF. Proposed lexicon for anatomic landmarks in normal posterior segment spectral-domain optical coherence tomography: the IN•OCT consensus. *Ophthalmology*. 2014;121:1572–1578.
29. Sadigh S, Cideciyan AV, Sumaroka A, et al. Abnormal thickening as well as thinning of the photoreceptor layer in intermediate age-related macular degeneration. *Invest Ophthalmol Vis Sci*. 2013;54:1603–1612.
30. Pfau M, von der Emde L, Dysli C, et al. Determinants of Cone and Rod Functions in Geographic Atrophy: AI-Based Structure-Function Correlation. *Am J Ophthalmol*. 2020;217:162–173.
31. Pfau M, von der Emde L, de Sisternes L, et al. Progression of Photoreceptor Degeneration in Geographic Atrophy Secondary to Age-related Macular Degeneration. *JAMA Ophthalmol*. 2020;138:1026–1034.
32. Schindelin J, Arganda-Carreras I, Frise E, et al. Fiji: an open-source platform for biological-image analysis. *Nature Methods*. 2012;9:676–682.
33. Vallat R. Pingouin: statistics in Python. *JOSS*. 2018;3:1026.
34. Nassisi M, Fan W, Shi Y, et al. Quantity of Intraretinal Hyperreflective Foci in Patients With Intermediate Age-Related Macular Degeneration Correlates With 1-Year Progression. *Invest Ophthalmol Vis Sci*. 2018;59:3431–3439.
35. Tiosano L, Byon I, Alagorie AR, Ji Y-S, Sadda SR. Choriocapillaris flow deficit associated with intraretinal hyperreflective foci in intermediate age-related macular degeneration. *Graefe's Arch Clin Exp Ophthalmol = Albrecht von Graefes Archiv fur klinische und experimentelle Ophthalmologie*. 2020;258:2353–2362.
36. Rogala J, Zangerl B, Assaad N, Fletcher EL, Kalloniatis M, Nivison-Smith L. In vivo quantification of retinal changes associated with drusen in age-related macular degeneration. *Invest Ophthalmol Vis Sci*. 2015;56:1689–1700.
37. Saßmannshausen M, Steinberg JS, Fimmers R, et al. Structure-function analysis in patients with intermediate age-related macular degeneration. *Invest Ophthalmol Vis Sci*. 2018;59:1599–1608.
38. Sevilla MB, McGwin G, Lad EM, et al. Relating retinal morphology and function in aging and early to intermediate age-related macular degeneration subjects. *Am J Ophthalmol*. 2016;165:65–77.
39. Pfau M, Lindner M, Gliem M, et al. Mesopic and dark-adapted two-color fundus-controlled perimetry in patients with cuticular, reticular, and soft drusen. *Eye (London, England)*. 2018;32:1819–1830.